Cancer Research

Inactivation of Cancer-Associated-Fibroblasts Disrupts Oncogenic Signaling in Pancreatic Cancer Cells and Promotes Its Regression

Patricia Dauer[1,2], Xianda Zhao[3], Vineet K. Gupta[1], Nikita Sharma[1], Kousik Kesh[1], Prisca Gnamlin[1], Vikas Dudeja[1], Selwyn M. Vickers[3,4], Sulagna Banerjee[1], and Ashok Saluja[1]

Abstract

Resident fibroblasts that contact tumor epithelial cells (TEC) can become irreversibly activated as cancer-associated-fibroblasts (CAF) that stimulate oncogenic signaling in TEC. In this study, we evaluated the cross-talk between CAF and TEC isolated from tumors generated in a mouse model of KRAS/mut p53-induced pancreatic cancer (KPC mice). Transcriptomic profiling conducted after treatment with the anticancer compound Minnelide revealed deregulation of the TGFβ signaling pathway in CAF, resulting in an apparent reversal of their activated state to a quiescent, nonproliferative state. TEC exposed to media conditioned by drug-treated CAFs exhibited a decrease in oncogenic signaling, as manifested by downregulation of the transcription factor Sp1. This inhibition was rescued by treating TEC with TGFβ. Given promising early clinical studies with Minnelide, our findings suggest that approaches to inactivate CAF and prevent tumor–stroma cross-talk may offer a viable strategy to treat pancreatic cancer.

Significance: In an established mouse model of pancreatic cancer, administration of the promising experimental drug Minnelide was found to actively deplete reactive stromal fibroblasts and to trigger tumor regression, with implications for stromal-based strategies to attack this disease. *Cancer Res; 78(5); 1321–33. ©2017 AACR.*

Introduction

Pancreatic cancer is one of the most devastating cancers with a dismal 5-year survival rate of less than 6% (www.cancer.gov; ref. 1). Recent studies suggest that the dense desmoplastic stroma, consisting of intense fibrosis, increased production of extracellular matrix (ECM), and proliferation of myofibroblast-like cells (2, 3), contributes to the aggressiveness and chemotherapeutic resistance, thereby leading to poor survival. This fibroinflammatory stroma, besides demonstrating multiple procancerous features, contributes to an increase in tumor interstitial fluid pressure thus inhibiting delivery of anticancer therapies to the tumor cells (4–6). However, stroma-targeted therapies have not been beneficial in terms of survival or prognosis (7). An ideal therapeutic regimen for pancreatic ductal adenocarcinoma (PDAC) would thus be a combination of antitumorigenic drugs that are minimally toxic, and anti-stromal to deplete the dense stroma and/or disrupt its cross-talk with the tumor cells (8, 9).

The PDAC stroma consists of activated fibroblasts, also known as cancer-associated fibroblasts (CAF), immune cells, vasculature, and an abundance of ECM proteins (10). This reactive milieu of cells modulates both tumor epithelial cells (TEC) and its microenvironment to promote tumor progression. CAFs secrete chemokines and cytokines that are protumorigenic and help the tumor proliferate and metastasize. While stromal cells do not exhibit the genetic transformations seen in malignant pancreatic cancer cells, they are altered by cytokines, and growth factors secreted by inflammatory cells and tumor cells (11, 12). In the initial phases of tumor development, stroma production is stimulated by cancer cell–derived growth factors including TGFβ, hepatocyte growth factor (HGF), fibroblast growth factor (FGF), and EGF (13). These tumor-derived factors and immune cell–derived factors activate the quiescent stellate cells in the pancreas and make them myofibroblast-like. During these transformations under the influence of the tumor, the activated stellate cells further transform to CAFs. In their activated state, CAFs secrete ECM components, primarily type I and III collagen, fibronectin, and proteoglycans. Till date, it has not been elucidated whether CAFs can revert to normal quiescent fibroblasts (14, 15).

Studies in our laboratory show that triptolide, a diterpene triepoxide from the Chinese plant *Tripterygium wilfordii*, induces cell death in pancreatic cancer cells, and is effective in reducing tumor growth and locoregional spread in several complementary models of pancreatic cancer (16). For ease of clinical application, we have developed a water-soluble prodrug, Minnelide, for this compound (17–22). Mechanistically, we have demonstrated that Minnelide downregulates HSP70 via inhibition of the activity of the transcription factor Sp1, thereby leading to pancreatic cancer cell death (23, 24). Our recent publications showed that in addition to being effective against the epithelial pancreatic cancer cells, Minnelide also depletes the stroma by preventing the

[1]Department of Surgery, University of Miami, Miami, Florida. [2]Department of Pharmacology, University of Minnesota, Minneapolis, Minnesota. [3]Department of Surgery, University of Minnesota, Minneapolis, Minnesota. [4]Department of Surgery, University of Alabama, Tuscaloosa, Alabama.

Note: Supplementary data for this article are available at Cancer Research Online (http://cancerres.aacrjournals.org/).

GenBank accession number: GSE74490.

Corresponding Authors: Ashok Saluja, Department of Surgery, PAP Research Building, University of Miami, 1550 NW 10th Ave, Miami, FL 33136. Phone 305-243-8448; Fax: 305-243-6263; E-mail asaluja@miami.edu; and Sulagna Banerjee, Sulagna.banerjee@med.miami.edu

doi: 10.1158/0008-5472.CAN-17-2320

synthesis of hyaluronan and collagen stabilization. Furthermore, treatment with Minnelide reduces the viability of CAFs isolated from the pancreatic tumors (6). Our preclinical studies show that at a dose of 0.4 mg/kg, Minnelide is an effective cytotoxic compound that targets multiple pathways in a tumor cell. At this dose, Minnelide eliminates stromal cells and decreases ECM components like collagen and HA, thereby relieving the pressure on blood vessels allowing them to be functional, which results in better drug delivery (6). Minnelide has just completed the phase I clinical trial against advanced gastrointestinal malignancies and is currently awaiting phase II trials. The phase I has yielded very encouraging results with significant tumor responses observed in terms of reduced tumor activity on PET-CT and many patients with partial response or stable disease (manuscript under preparation; ref. 25). This phase I trial revealed that the MTD for Minnelide is 0.67 mg/m^2. This roughly translates to 0.2 mg/kg in mice. At this dose, Minnelide depletes the stromal ECM, resulting in relieving the interstitial pressure on the blood vessels and leading to better drug delivery (6).

In this study, we performed an exhaustive transcriptome analysis on CAFs and determined that the profound effect of Minnelide on the pancreatic tumor stroma is due to inactivation of CAFs in the tumor. This further results in a low ECM production via suppression of the TGFβ signaling pathway in CAFs. Inactivation of CAFs leads to a decreased "cross-talk" between the tumor and the stroma, leading to decreased oncogenic signaling, suppressed tumor growth, and invasion.

Materials and Methods

Cell lines and cell culture

Four primary cell lines were isolated from Kras^{G12D}; Trp53^{R172H}; Pdx-1-Cre (KPC) mice. The TECs were isolated according to our previous study (22). Isolation of CAFs (CAF-1, CAF-5 and CAF-7) from three KPC mice was performed following the protocol described by Sharon and colleagues (26). The purity of fibroblasts was checked by flow cytometry after staining isolated fibroblasts with fibroblast surface protein (FSP) antibody and CK19 antibody. Population with FSP+CK19– staining was used for downstream experiments. All the established cell lines were used between passages 5 and 18. We also used three preestablished cell lines, the mouse PDAC cell line Panc02, and the human PDAC cell line S2-VP10 (gift from Dr. Masato Yamamoto's laboratory, University of Minnesota, Minneapolis, MN) and the human pancreas fibroblasts SC00A5 (Vitro Biopharma). KPC-1 and CAFs were maintained in DMEM (Gibco, Thermo Fisher Scientific) containing 10% FBS and 1% penicillin/streptomycin (Gibco). Panc02 and S2-VP10 were cultured in RPMI1640 (Gibco) containing 10% FBS and 1% penicillin/streptomycin (Gibco). SC00A5 was maintained in MSC-GRO Low serum, Complete Media (Vitro Biopharma). All cell lines were routinely tested for mycoplasma and STR profiles (ATCC).

FACS analysis

Single-cell suspensions were prepared from fresh cell culture. Cell fixation and permeabilization was performed with the BD Biosciences Cytofix/Cytoperm kit (BD Biosciences), according to the manufacturer's instructions. Apoptosis and bromodeoxyuridine (BrdUrd) incorporation for proliferation was done using Apoptosis and Cell Proliferation Kit following manufacturer's instructions (BD Biosciences). Analysis of αSMA, TGFβ receptor type 1, and TGFBR2 (Abcam) were conducted by FACS. All samples were analyzed on BD FACSCANTO II flow cytometers (BD Biosciences). Data was acquired and analyzed with FACSDiVa software (BD Biosciences) and FlowJo Software.

Invasion assay

Tumor cell invasion was measured by counting the number of tumor cells that invaded through Matrigel precoated transwell chambers with 8-mm pores (BD Biosciences). On the top of inserts: 24-hour FBS starved, untreated, or 100 nmol/L 24-hour triptolide-treated tumor cells (KPC-1, Panc02 and S2-VP10, 1.5×10^5 each) were placed. On the bottom chamber, untreated or 100 nmol/L 24-hour triptolide-treated CAFs (CAF-1, CAF-5 and SC00A5, 1.5×10^5 each) in 1% FBS were added. The negative control group was added with 1% FBS in the bottom chamber. After incubation for 24 hours (KPC-1 and S2-VP10) to 48 hours (Panc02) for invasion, the invaded cells were fixed with 70% ethanol, stained with crystal violet, and 5 random fields were counted under a light microscope. Each experiment was repeated thrice.

Production of conditioned media

Conditioned media (CM) of tumor cells and CAFs was produced using FBS-free basal media to exclude the effects of growth factors in serum for downstream experiments. In normal conditions, 70% confluent cells were cultured in FBS-free basal media for 48 hours. In experiments designed to analyze the effects of triptolide, 100% confluent cells were cultured in FBS-free basal media containing 25 nmol/L triptolide for 24 hours and then changed to no drug, FBS-free, basal media for 48 hours. The resulting CM were centrifuged for 10 minutes at 1,000 rpm after collection and stored at −80°C for no more than two months before use.

Measurement of ECM and TGFβ secretion

To evaluate the effects of triptolide on ECM secretion of CAFs, we measured concentration of total collagens, fibronectin (FN), periostin, hyaluronic acid (HA), matrix metallopeptidase 2 (MMP2), and MMP9 in CM derived from CAFs. ELISA was used to quantify FN (BioVision), periostin (Thermo Scientific), HA (TSZELISA), MMP2 (Abcam), and MMP9 (Abcam). Total collagen was quantified by Sircol collagen assay kit (Biocolor Life Science Assays). Meanwhile, autocrine signaling of TGFβ1 (Abcam) and TGFβ2 (R&D Systems) were determined by ELISA in CM. All the experiments were performed according to the manufacturer's protocol.

Animal model

All animal experiments were performed according to the University of Miami Animal Care Committee guidelines. Both transgenic mouse model of spontaneous PDAC and orthotopic PDAC mouse model were included. KPC animals were generated by crossing Lox-Stop-Lox (LSL) KRas^{G12D}; Trp53^{R172H} animals with Pdx-1 Cre animals. Minnelide treatment with 0.2 mg/kg body weight was started when animals were 8 weeks of age. Animals in saline and treatment groups were age-matched. After 30 days of Minnelide treatment, animals were sacrificed and tumor tissues were collected. For one arm of orthotopic PDAC mouse model, 1,000 KPC-1 cells were suspended in Matrigel (BD Biosciences) and injected in the pancreas of 20 C57BL/6 mice, for another arm, 1,000 KPC-1 cells plus 9,000 CAF-1 cells were suspended in Matrigel (BD Biosciences) and injected in the pancreas of 20

C57BL/6 mice. Ten mice from each arm were treated with Minnelide (0.2 mg/kg body weight) for 30 days before sacrifice.

Immunofluorescence and IHC

For immunofluorescence, 4-μm paraffin tissue sections were deparaffinized in xylene and rehydrated through graded ethanol. Hematoxylin and eosin (H&E) staining were conducted to confirm histologic features. Primary antibodies for αSMA (Abcam), cleaved-PARP (Abcam), FN (Santa Cruz Biotechnology), and vimentin (Cell Signaling Technology) were diluted according to the manufacturer's instruction and incubated overnight at 4°C. The primary antibody was omitted for the negative controls. Alexa Fluor–conjugated secondary antibody (Invitrogen) were used for visualizing. Slides were counterstained with DAPI and observed in a Leica fluorescent microscope. IHC was used to detect BrdUrd in tissue sections according to manufacturer's protocol (Abcam).

Sirius red staining and measurements

Tissue sections were stained using picrosirius red staining solution (Chondrex Inc) according to the manufacturer's instructions. The Sirius red–stained area was quantified using ImageJ software by selecting stained fibers in five fields at a magnification of ×100 under a light microscope.

Quantitative real-time PCR assay

Messenger RNA (mRNA) expression was analyzed through qRT-PCR using LightCycler 480 System (Roche) and SYBR Green (Qiagen). The 18s ribosomal RNA expression was used to normalize the results obtained in different conditions. Primers used in this article were listed in Supplementary Table S1.

Transcriptome deep sequencing and analysis

Aliquots of RNA were derived from the qRT-PCR samples. CAF-1, CAF-5, and CAF-7 control group, triptolide short-term treatment group, and long-term treatment group were analyzed. The RNA was quality tested using a Bioanalyzer 2100 (Agilent Technologies). cDNA was created by reverse transcription of oligo-dT–purified polyadenylated RNA and fragmented, blunt-ended, and then ligated to barcoded adaptors. Then, the library was size selected, and the selection process was validated and quantified by capillary electrophoresis and qPCR, respectively. Samples were load on the HiSeq 2500 (Illumina Inc.) to generate around 25 million paired-end 50-bp reads for each sample.

Quality control was conducted by FastQC 0.11.2 according to http://www.bioinformatics.babraham.ac.uk/projects/fastqc (27). TopHat 2.0.5, was used to map the paired reads to the UCSC mm10 assembly of the mouse genome (28). The mean inner distance was established using the insertion size metrics feature of Picard tools. The resulting TopHat data served as input to other Cufflinks tools 2.2.0 (29). Transcripts were also assembled using Cufflinks, with stipulating the reference transcriptome Mus_musculus. GRCm38.74. All cufflinks assemblies were merged with Cuffmerge. Differentially expressed genes (DEG) were calculated with Cuffdiff and presented the data in terms of fragments per kilobase of transcript per million mapped reads (FPKM). Visualization of data from Cuffdiff outputs was used CummeRbund v2.0.0 (30), clusterProfiler (31), and Ingenuity Pathway Analysis (Qiagen) were used for pathway enrichment analysis. Gene-set enrichment analysis (GSEA; ref. 32) was conducted using app from http://www.broadinstitute.org/gsea/index.jsp. Raw data files and processed expression files are available online in the Gene Expression Omnibus at http://www.ncbi.nlm.nih.gov/geo/ (GenBank Accession Number: GSE74490).

Estimation of active and total TGFβ in the cells and media

CM from TECs (MIA-PaCa2 and S2-VP10) and activated pancreatic stellate cells (PSC) were collected after 48 hours of plating. Cell lysates from the TECs and PSCs were prepared by lysing the cells in RIPA buffer. Total and active TGFβ was estimated in the media and cell lysate using Legend Max TGF-β1 ELISA Kit and Legend Max Free Active TGF-β1 ELISA Kit (Biolegend).

Vitamin A accumulation assay

A total of 5,000 CAF-7 cells were plated in each well of a black 96-well plate with clear bottom. The following day, cells were either left untreated or treated with 25 nmol/L triptolide for 48 hours. After treatment, 10 ng/mL TGFβ was added for 30 minutes to two untreated rows (12 wells), and two rows treated with triptolide (12 wells). After 30 minutes, cells were washed gently with PBS, and phenol-free media were replaced. Fluorescence was measured with excitation of 300 nm and emission of 338 nm on half of the plate. The other half of the plate was used for determining viability, as described previously.

Oil red staining

A total of 2×10^4 CAF-7 cells were plated in each well of a four-well chamber slide. The following day, two wells were treated with 25 nmol/L triptolide for 48 hours. After treatment, 10 ng/mL TGFβ was added for 30 minutes to one untreated well, and one well treated with triptolide. Cells were then washed gently with PBS, and fixed with 2% paraformaldehyde for 30 minutes. Cells were washed with water, and incubated with 60% isopropanol/40% water for 5 minutes. Sixty percent isopropanol was removed, and replaced with Oil Red O working solution (3 parts Oil Red O:2 parts water) for 20 minutes. Cells were again washed with water, and counterstained with hematoxylin for 1 minute. Cells were washed, mounted with permount, and imaged with a light microscope.

Sp1 activity assay

Human pancreatic stellate cells (hPSC) were seeded in four, 10-cm plates, and cultured until 70%–80% confluent, and were then treated with 25 nmol/L triptolide for 48 hours. Meanwhile, 3×10^5 MIA PaCa-2 and S2-VP10 cells were seeded in 6-cm plates. After 48 hours, 10 ng/mL TGFβ was added to one untreated hPSC plate and one triptolide-treated hPSC plate for 30 minutes. The CM from the hPSCs was collected. Any DMEM on the MIA PaCa-2 cells was removed and the cells were rinsed with PBS. Conditioned media from the hPSCs was added to the MIA PaCa-2 cells for an additional 24 hours as follows: untreated hPSCs, hPSC + TGFβ, hPSC + triptolide, and hPSC + triptolide + TGFβ. Cell lysates were collected for each sample and added in duplicate to the Sp1 TransAM ELISA plate (Active Motif). The ELISA was performed per the manufacturer's instructions, and the Sp1 binding was normalized to protein concentration.

Dual luciferase reporter assay

MIA PaCa-2 and hPSCs were plated at a density of 8×10^4 cells per well in a 24-well plate. Cells were treated with triptolide (25 nmol/L for 48 hours) and TGFβ (10 ng/mL for 30 minutes). The supernatant from hPSCs treated with triptolide was plated on top of the MIA PaCa-2 cells. After 48 hours of the hPSC conditioned

media on MIA PaCa-2 cells, the cells were lysed with 1× Passive lysis buffer. The plate was then kept at −80°C overnight and the luciferase activity was measured the next day using the stop and glow kit from Promega according to the manufacturer's protocol.

Electric cell-substrate impedance sensing

CAF-7 proliferation was measured by electric cell-substrate impedance sensing (ECIS). CAF-7 cells were seeded in 8W10E+ PET arrays with or without TGFβ (10 ng/mL) and or triptolide (25 nmol/L). Impedance (Z), capacitance (C), and resistance (R) were monitored for 60 hours by an ECIS Model ZΘ instrument (Applied BioPhysics Inc.) and normalized to Z_0.

Statistical analysis

Values are expressed as the mean ± SEM. Two-group data were analyzed using a *t* test. Multigroup data were first analyzed using one-way ANOVA, if there are positive findings; Bonferroni multiple comparisons test was performed to finish pairwise comparisons. A $P < 0.05$ was considered statistically significant.

Results

Low-dose Minnelide decreased CAF-induced tumor growth in pancreatic cancer animal model

It is well established that CAFs promote tumor development and invasion in number of cancers. To evaluate the effects of triptolide (the active compound of Minnelide) on TEC invasion in the presence and absence of CAFs, a Boyden chamber assay was conducted. Three cell line pairs, CAF-1/Panc02, CAF-5/KPC-1, and SC00A5/S2-VP10 were set up (Fig. 1A–C). CAFs increased invasion rate in untreated-tumor cells from 2- to 4-fold. Interestingly, when CAFs were treated with triptolide before coculture with tumor cells, their invasion inducing roles decreased dramatically compared with untreated CAFs (Fig. 1A–C). Inhibition of invasion of CAFs on TECs was similar to that observed when TECs were treated with same dose of triptolide. In addition to promoting invasion, the untreated CAFs also induced tumor cell growth (Supplementary Fig. S1A and S1B). These results demonstrated that tumor growth and invasion-promoting functions of CAFs were impaired by triptolide.

To see whether Minnelide affected CAF-induced tumor burden at a low dose (within the MTD of 0.67 mg/m^2 that is equivalent to 0.2 mg/kg in mice), *in vivo* we coinjected CAF: TEC (9:1) orthotopically in the pancreas of C57/Bl6 mice ($n = 8–9$). Animals were treated with 0.2 mg/kg Minnelide for 30 days. Tumor weight was measured at the completion of the experiment. Our results showed that the presence of CAF cells generated larger tumors compared with those that did not have CAF cells injected (Fig. 1D). When treated with Minnelide, tumors having CAF cells showed greater decrease in tumor weight compared with those that did not have CAFs ($P = <0.05$). Furthermore, Minnelide treatment resulted in decreased collagen in the tissue and decreased αSMA expression (Fig. 1E; Supplementary Fig. S2A and S2B). TUNEL staining indicated increased apoptosis in the group with CAF/TEC treated with Minnelide compared with the TEC alone treated with Minnelide. Furthermore, decreased BrdUrd staining indicated decreased proliferation was observed in the CAF/TEC group compared with the TEC group alone (Fig. 1E; Supplementary Fig. S2C). Upon scoring the metastatic lesions, we observed that the group having TEC had a 37.5% metastatic index, which, when treated with Minnelide, was reduced to 22.2%. However, the TEC/CAF group had a higher metastatic index (75%), which was decreased to 44.4% upon treatment with Minnelide (Fig. 1F). This indicated that presence of CAFs in a tumor increased proliferation of the TECs, production of collagen, and expression of αSMA. Upon treatment with 0.2 mg/kg Minnelide, both group responded equally to the compound and decreased the collagen secretion, αSMA secretion, proliferation, and increased the apoptosis in these cells.

In the KPC mouse model that fully recapitulates disease progression of human PDAC, we measured the amount of desmoplastic markers, such as collagen, FN, and the cellular component fibroblasts, in response to Minnelide treatment. Heavy desmoplasia was seen in KPC mice without Minnelide treatment, while in the Minnelide treatment group, less collagen. and FN were expressed (Supplementary Fig. S3A–S3I).

Transcriptomic analysis of CAFs after triptolide treatment

To study which pathways in CAFs were being downregulated by triptolide, we next conducted a transcriptome analysis based on RNA-Seq. Cell lines CAF-1, CAF-5, and CAF-7 were either untreated or treated with triptolide (100 nmol/L) for 6 hours or 24 hours. All samples had around 25 million paired reads with over 90% mapped uniquely mapped (Supplementary Table S2). A total of 3,859 DEGs were identified between control group and triptolide 24-hour group with a FDR of 0.05 (Fig. 2A and B). To further analyze the pathways that are deregulated by triptolide, we conducted pathway enrichment analysis and found that most significantly downregulated pathways were the RAR/RXR signaling pathway and TGFβ signaling (Fig. 2C). Interestingly, RAR/RXR pathway is a retinoic acid (RA) stimulated pathway. In the presence of RA, which is a morphogen derived from vitamin A, RA translocates to the nucleus and stimulates the RAR/RXR to bind to their response elements (RARE), resulting in transcription of genes that regulate differentiation, survival, and TGFβ secretion. Our analysis showed that several genes in this pathway were being differentially regulated (Supplementary Fig. S4A and S4B).

IPA analysis showed that TGFβ signaling pathway was significantly downregulated in CAFs (Fig. 2D). Furthermore, the downstream genes of TGFβ signaling pathway were also downregulated in triptolide-treated group (Fig. 2E and F). The top ten up- and downregulated genes are tabulated in Supplementary Fig. S4C. Interestingly, in the TECs, these pathways were not among the top significant pathways that were deregulated (data not shown).

Triptolide downregulated the TGFβ pathway in CAFs at a sublethal dose

It is well known that upon activation, the stromal cells, specifically fibroblasts, secrete TGFβ. Our results confirmed this (Fig. 3A and B). As our transcriptomics analysis was done at a dose of 100 nmol/L triptolide, we next studied the effect of low dose of triptolide on the TGFβ signaling. We treated the CAFs with a very low dose of 25 nmol/L triptolide and analyzed all the components of the TGFβ pathway. Our study showed that the autocrine TGFβ signaling pathway in the CAFs was downregulated even at 25 nmol/L tritptolide. The expression of TGFβ was significantly decreased both at the RNA level (Fig. 3C) as well as secretion level in both cells and supernatant (Fig. 3D and E). In addition, effectors of TGFβ pathway (SMAD2–4) were downregulated both at the RNA (Fig. 3F) and protein level (Fig. 3G). In addition, several other genes that were directly being regulated by the TGFβ signaling were also downregulated (Fig. 3F). The expression and secretion of the TGFβ, as well as all its components

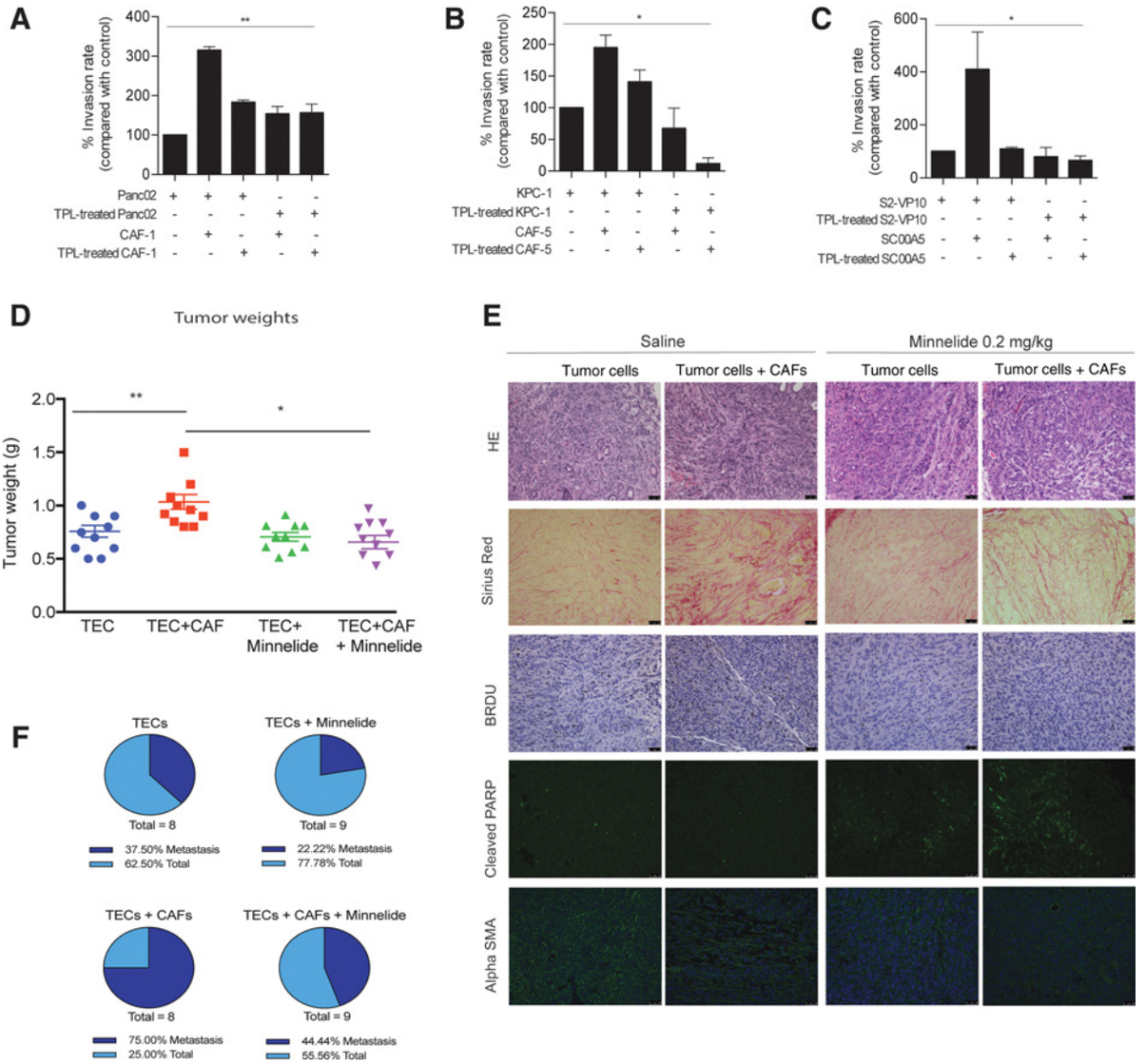

Figure 1.

Triptolide/Minnelide inhibited CAF-mediated invasion, tumor development, and desmoplasia of TECs in pancreatic cancer cells and animal model. **A–C,** Coculture of TEC (mouse-derived KPC, Panc-1, or human-derived S2-VP10) with CAF cells (mouse-derived CAF-1, CAF-5 or human-derived SC00A5) resulted in increased invasion in a Boyden chamber, which was decreased upon treatment with 25 nmol/L triptolide of CAF cells, TECs, or both. **D,** Coinjection of CAFs with tumor cells increased tumor growth in orthotopic PDAC mouse model, but Minnelide treatment suppressed tumor-promoting roles of CAFs *in vivo*, as can be seen by the end of study tumor weight. Analysis of tumors by H&E staining, sirius red staining, and BrdUrd staining showed that CAFs induced increased collagen synthesis and proliferation in TECs; however, this was decreased upon treatment with Minnelide. **E,** Minnelide also induced apoptosis, as seen by cleaved PARP staining and TUNEL staining. **F,** Although CAFs promoted metastasis, treatment with Minnelide resulted in decreased metastatic lesions, as can be observed by the metastatic index. In summary, Minnelide suppressed CAF-mediated collagen deposition, cell proliferation, metastasis, and αSMA and induced apoptosis in orthotopic PDAC model. (*, $P < 0.05$; **, $P < 0.01$).

that were decreased by triptolide treatment were rescued when treated with recombinant TGFβ (Fig. 3F and G).

Downregulation of TGFβ pathway in CAFs reverted them from activated to inactivated state

Activation of PSCs is characterized by loss of vitamin A droplets in these cells and a subsequent increase in αSMA expression. Thus, an increase in vitamin A and lipid droplet accumulation in the fibroblast as well as a loss of αSMA would indicate an inactivation of CAFs. We observed that treatment with triptolide decreased proliferation of CAFs without affecting their viability (Fig. 4A). To study whether this was due to "inactivation" of CAFs, we next analyzed the vitamin A droplets in these cells after treatment with triptolide. Our results showed that treatment with triptolide increased vitamin A accumulation (seen by monitoring fluorescence at 338 nmol/L) in CAFs. Interestingly, upon treatment with TGFβ in the presence of triptolide, the vitamin A fluorescence decreased to that observed in untreated cells

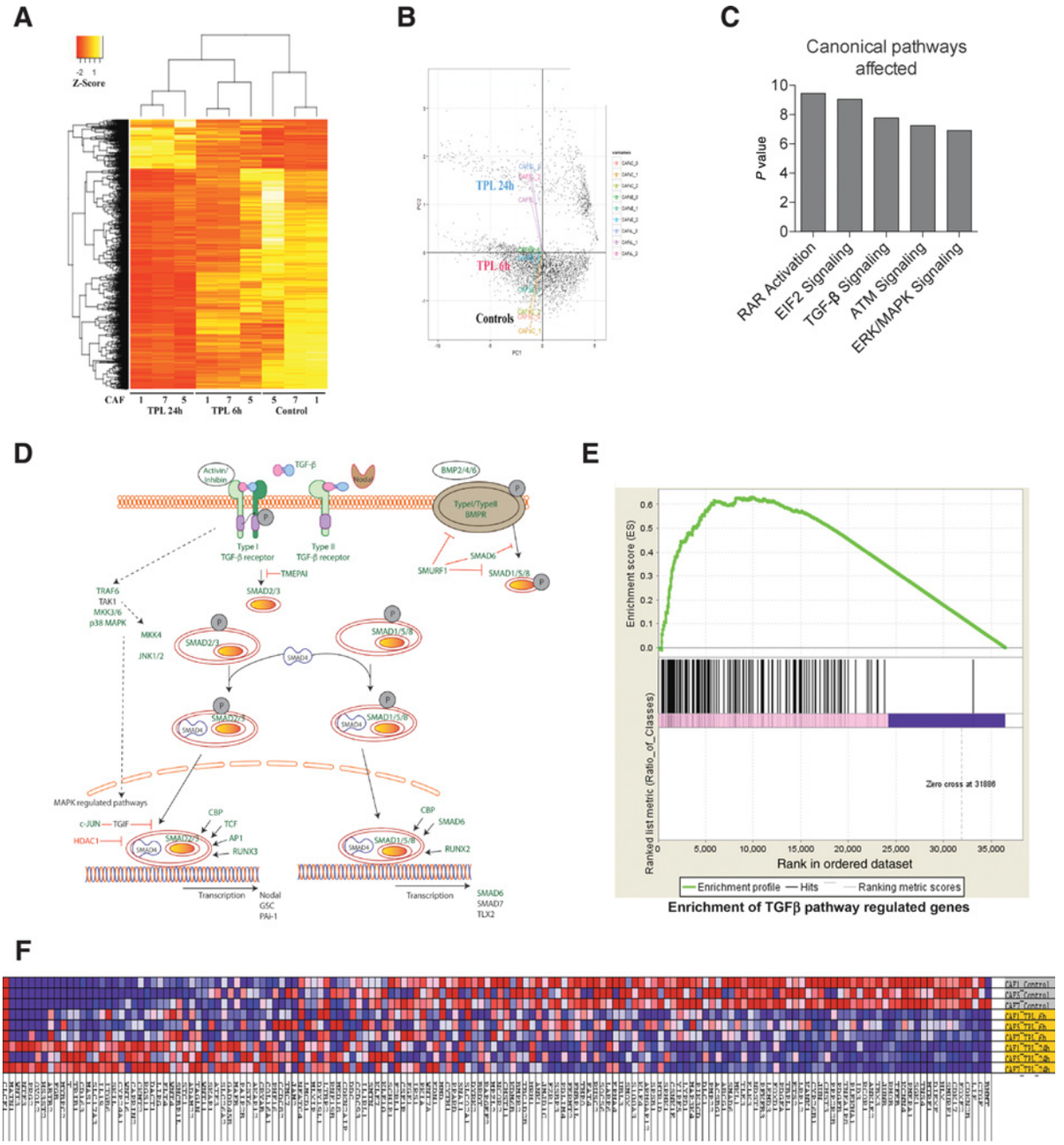

Figure 2.

Transcriptome analysis of triptolide-treated CAFs. **A,** Differentially expressed genes in CAFs before and after triptolide treatment were shown in heatmap. **B,** Principal component analysis showed three distinct groups of all samples that correlate to different treatments. **C,** Pathways that were significantly deregulated in 24-hour triptolide treatment samples are shown as a bar plot. **D,** Visualization of TGFβ pathway in response to triptolide treatment in CAFs. Green labels, downregulated genes; red-labels, upregulated genes. **E,** GSEA indicated obvious suppressive role of triptolide on TGFβ pathway downstream genes' expression. **F,** Heatmap of TGFβ pathway downstream genes' expression before and after triptolide treatment. Red, high expression; blue, low expression.

(Fig. 4B). This indicated that TGFβ was capable of reverting the triptolide-induced inactivation. This was further supplemented by our IPA analysis of the RAR/RXR pathway. We observed an increased expression of RBP (Retinol Binding Protein) in our triptolide-treated CAFs (Supplementary Fig. S4A). RBP is required for stabilization of retinol in the cells, thus, this further conformed to our hypothesis that triptolide was indeed inactivating the CAFs, resulting in accumulation of vitamin A. To confirm this observation further, we next performed an Oil Red staining on the CAF cells. We observed an increased Oil Red stain in the triptolide-treated CAFs, which decreased upon treatment with TGFβ (Fig. 4C).

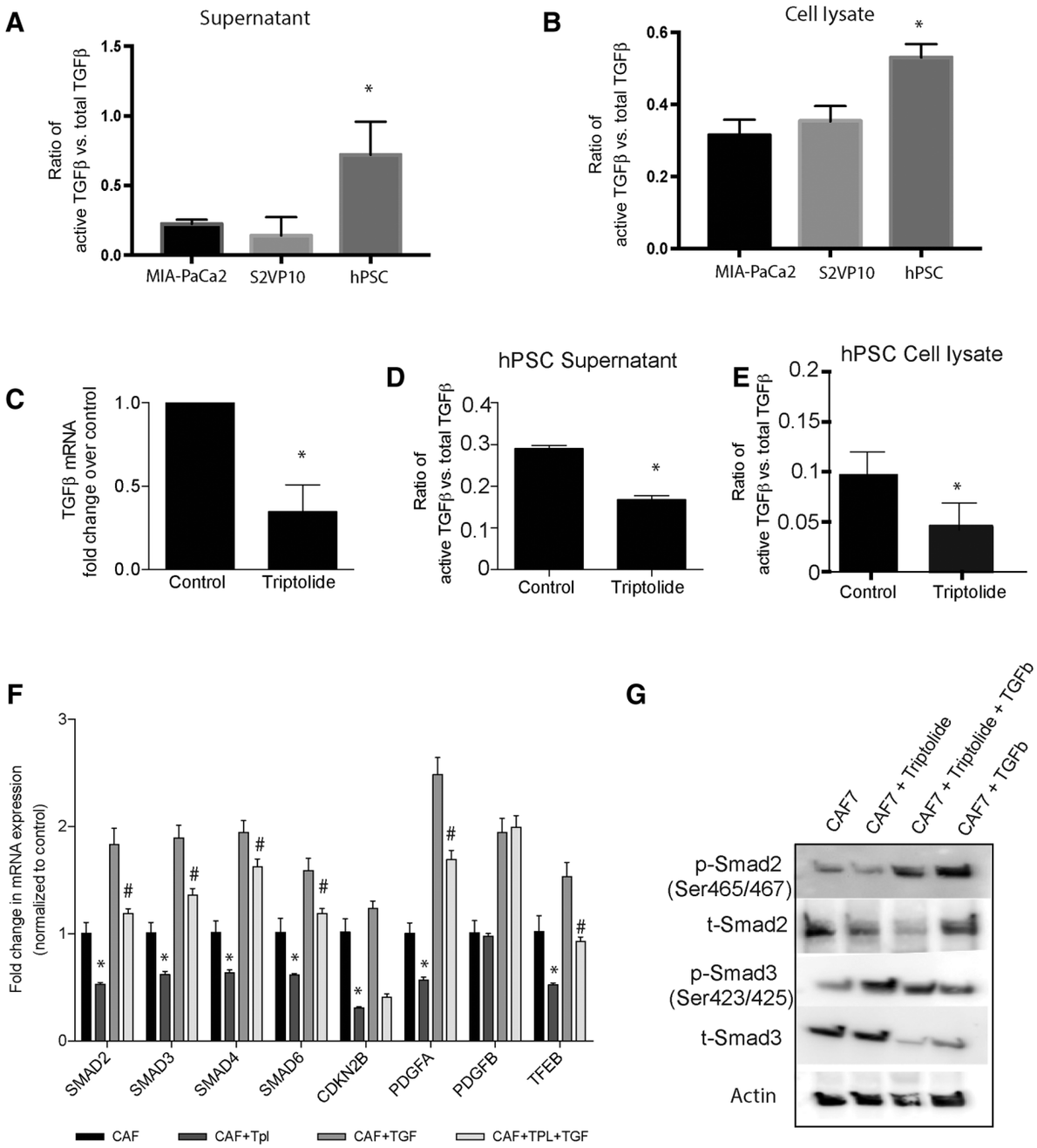

Figure 3.

Triptolide downregulated TGFβ pathway in the CAFs. **A** and **B,** Activated PSCs produced more active as well as total TGFβ compared with the TECs in culture supernatant (**A**) as well as in the cell lysate (**B**) as seen by the ratio of the active:total TGFβ. Treatment with 25 nmol/L triptolide (sublethal) decreased mRNA expression (**C**) as well as active:total TGFβ in hPSC supernatant (**D**) as well as cell lysate (**E**). **F,** mRNA expression of several genes in the TGFβ pathway was downregulated by triptolide treatment of activated PSCs. This was rescued by the addition of recombinant TGFβ. **G,** Triptolide treatment also downregulated the activity of SMAD2 and SMAD3 proteins, as seen by decreased phosphorylation in Western blot analysis. This was rescued by addition of recombinant TGFβ. *, $P < 0.05$ in control versus triptolide treatment; #, $P < 0.05$ in triptolide-treated versus TGFβ + triptolide-treated samples.

αSMA is a classic marker for activation of PSCs. When in their quiescent state, PSCs do not express αSMA. However, upon activation, this protein is upregulated. Treatment of CAF cells with triptolide decreased the αSMA+ cells as seen by flow cytometry (Fig. 4D).

To study whether treatment with triptolide is affecting the other functions of CAFs as well, we next analyzed their ECM secretion. Our results showed that treatment with 25 nmol/L triptolide decreased the secretion of fibronectin (Fig. 5A), periostin (Fig. 5B), collagen (Fig. 5C), hyaluronic

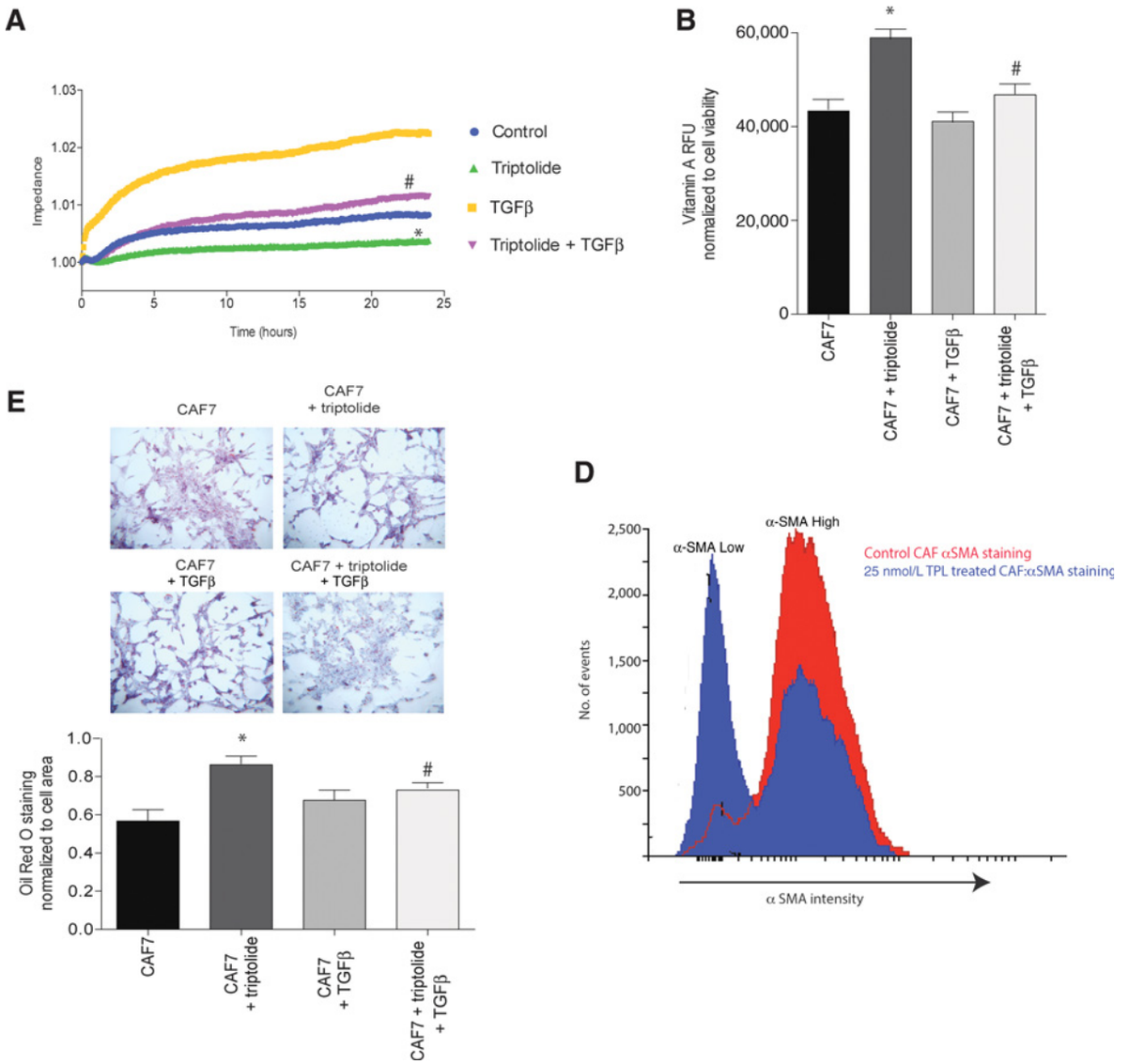

Figure 4.

Downregulation of TGFβ pathway in CAFs by triptolide reverts them from activated to inactivated state. **A–C,** Treatment of TEC (KPC001) with CM from CAF7 treated with 25 nmol/L triptolide decreased proliferation rate of KPC001 as measured by ECIS (**A**), resulted in vitamin A accumulation as observed by change of fluorescence at 338 nmol/L (**B**) and lipid droplet accumulation by Oil Red staining (**C**). Furthermore, analysis αSMA expression by flow cytometry showed a decrease in the intensity of staining, indicating an inactivation of CAF cells in the presence of triptolide (**D**). *, $P < 0.05$ in control versus triptolide treatment; #, $P < 0.05$ in triptolide-treated versus TGFβ + triptolide-treated samples.

acid (Fig. 5D), MMP2 (Fig. 5E), and MMP9 (Fig. 5F). Furthermore, treatment with TGFβ reverted this decreased ECM production (Fig. 5G and H).

Decreased TGFβ signaling in CAFs affected oncogenic signaling in tumor epithelial cells

It is well established that the tumor–stroma cross-talk is involved in tumor progression and metastasis. As our data indicated that triptolide decreased the TGFβ signaling in the CAF cells and also induced inactivation, we next studied the effect of this inactivation on the TECs. Our previously published data showed that Sp1 was one of the transcription factors that was overexpressed in pancreatic cancer, and this in turn upregulated the antiapoptotic pathways and proteins like NFκB pathway and HSP70. To study whether the decreased TGFβ from the "inactivated" CAFs decreased these pathways, we used the next set of CM from activated PSC cells (+/− triptolide) and added it to MIA PaCa-2 cells. In a parallel set, we added 10 ng/mL TGFβ to the MIA PaCa-2 cells with CM from 25 nmol/L triptolide -treated PSC cells. A dual luciferase reporter assay for SMAD showed that the CM from triptolide-treated PSCs downregulated the SMAD transcriptional activity, which was rescued in the presence of TGFβ (Fig. 6A). As SMAD transcriptional activity leads to transcription of Sp1 (33–35), we next tested the *Sp1* gene expression and

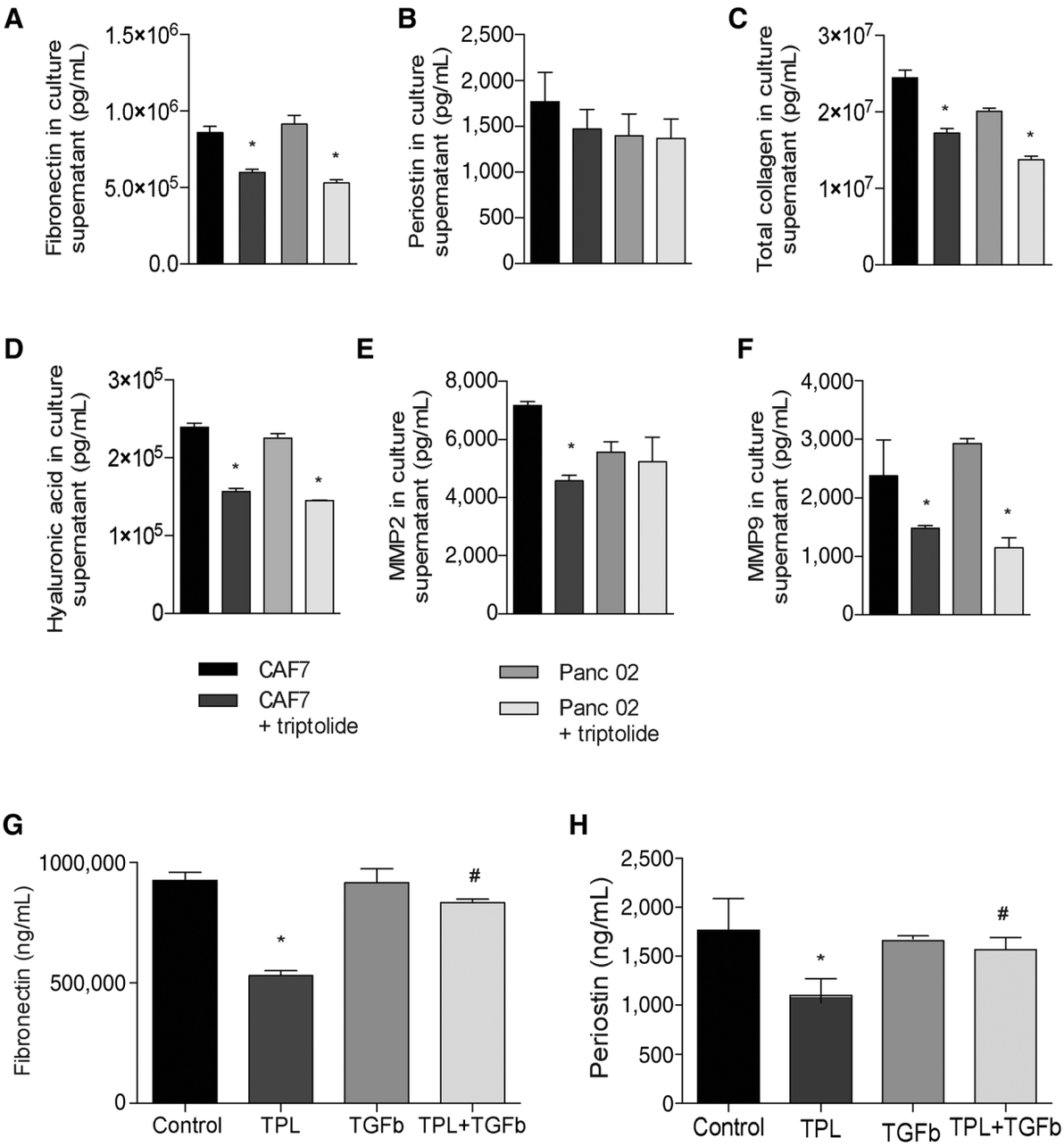

Figure 5.

Treatment with triptolide decreased ECM secretion by CAFs. Treatment with 25 nmol/L triptolide decreased the secretion of fibronectin (**A**), periostin (**B**), collagen (**C**), hyaluronic acid (**D**), MMP2 (**E**), and MMP9 (**F**). Furthermore, treatment with TGFβ reverted this decreased ECM production (**G** and **H**). *, $P < 0.05$ in control versus triptolide treatment; #, $P < 0.05$ in triptolide-treated versus TGFβ + triptolide-treated samples.

activity. Our results showed that Sp1 mRNA expression was downregulated in the set with conditioned media from 25 nmol/L triptolide. This expression was subsequently rescued upon adding TGFβ to the MIA PaCa-2 cells (Fig. 6B). We next studied the effect of CAF inactivation on Sp1 DNA binding and transcriptional activity. Our results showed that in the presence of CM from the 25 nmol/L triptolide-treated PSC, Sp1 binding was significantly decreased (Fig. 6C), indicating that CAF inactivation led to inhibition of transcriptional activity as well. Treatment with TGFβ reverted the Sp1 DNA binding, confirming that this inhibition of DNA binding was mediated via downregulation of TGFβ secretion by the PSCs. Our previously published data show that in the TECs, Sp1 downregulation inhibits antiapoptotic proteins like NFκB and HSP70. To study whether inactivation of PSCs also led to this phenotype, we studied the HSP70 and NFκB gene expression after treating cancer cells with CM from

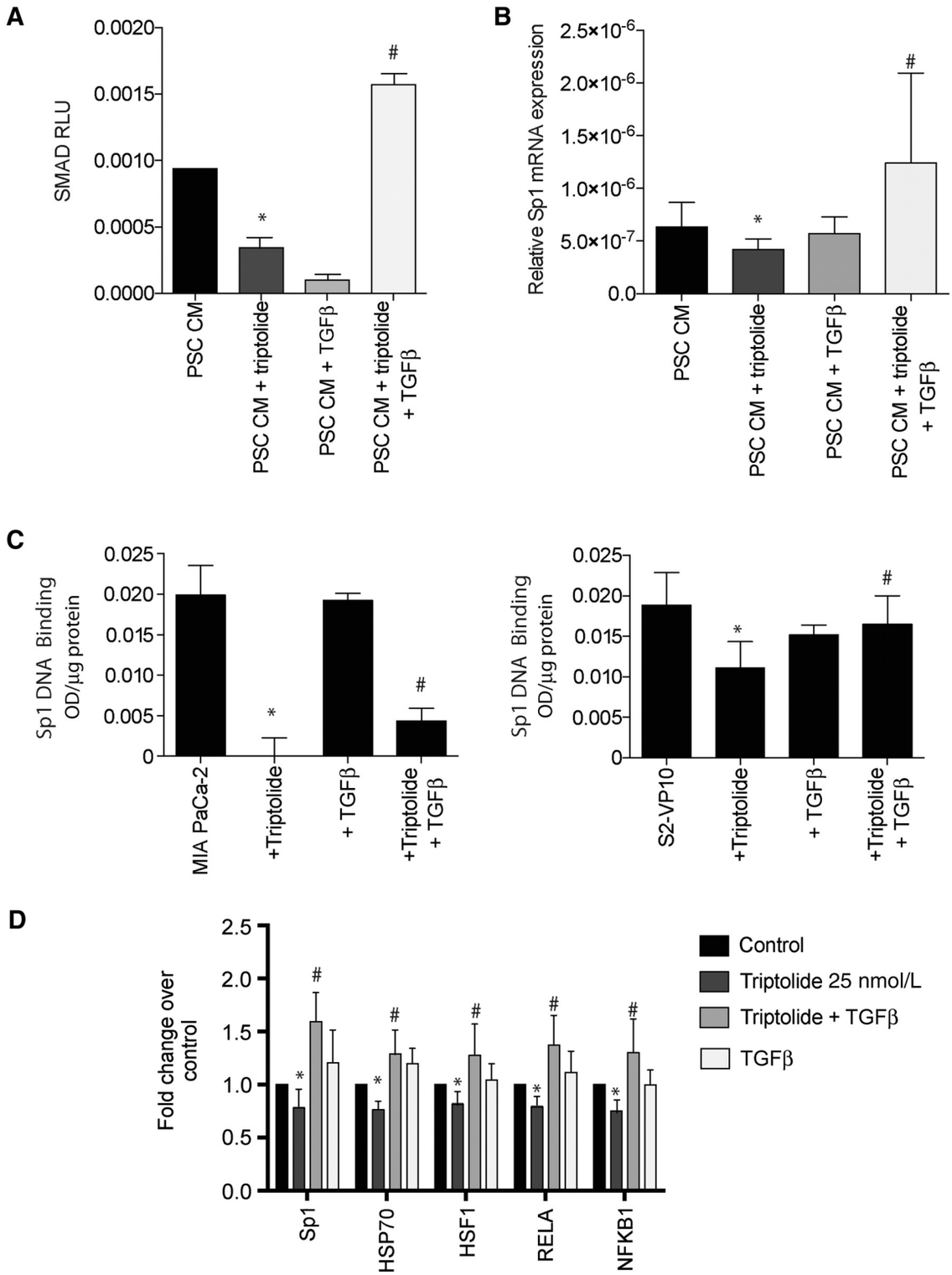

Figure 6.

Downregulation of TGFβ in CAFs inhibits oncogenic signaling in TECs. **A,** Treatment of TEC (MIA-PACA2 or S2-VP10) with CM from activated PSCs treated with 25 nmol/L triptolide decreased SMAD transcriptional activity, as seen by dual luciferase assay. This resulted in decreased Sp1 expression in the TECs (**B**). Furthermore, DNA-binding ability of Sp1 was inhibited (**C**). Expression of genes downstream of *Sp1* like *HSP70*, *HSF1*, and components of NFκB pathway (*RelA* and *NFKB1*) were also downregulated. These were rescued upon addition of recombinant TGFβ (**D**). *, $P < 0.05$ in control versus triptolide treatment; #, $P < 0.05$ in triptolide-treated versus TGFβ + triptolide-treated samples.

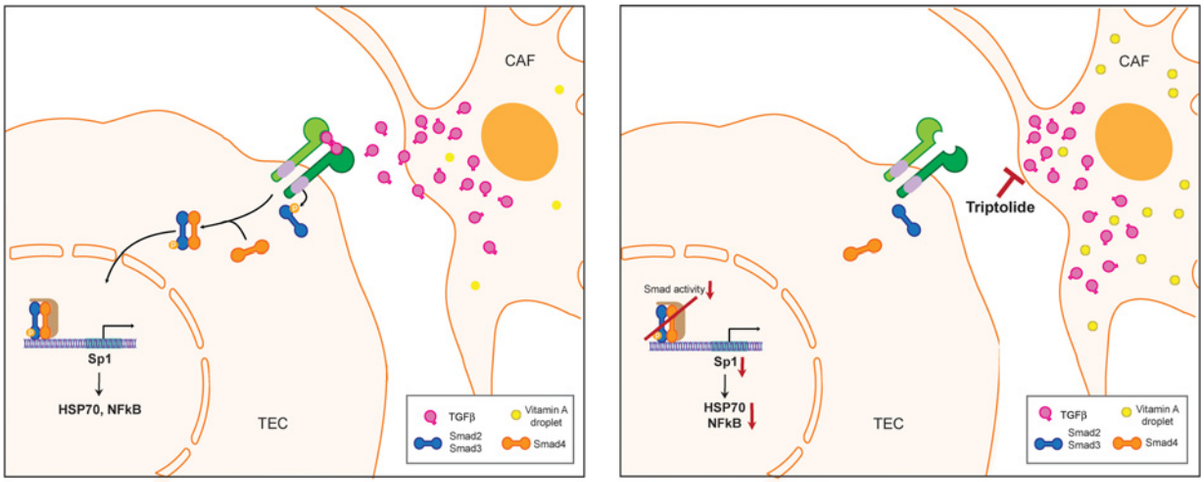

Figure 7.
Schematic figure illustration of how Minnelide-mediated inactivation of CAFs affects oncogenic signaling in TECs. Minnelide inactivates the CAF cells, leading to decreased production of TGFβ, which in turn downregulates pro-oncogenic signaling in the tumor epithelial cells.

25 nmol/L triptolide. Our results showed that MIA PaCa-2 cells treated with CM from PSCs plus triptolide downregulated p50 and p65 expression, and adding TGFβ upregulated expression, when compared with untreated PSC CM (Fig. 6D).

Discussion

Pancreatic tumors are characterized by a robust desmoplastic stroma, a significant part of which is comprised of myofibroblast-like cells. The origin of these cells remains unclear but a substantial part of these cells are derived from PSC. These cells are very similar to those found in the liver (hepatic stellate cells, HSC), which have been well studied in context of liver injury. In a normal pancreas, the PSCs are a quiescent population typically characterized by the presence of a large amount of vitamin A droplets or retinol (36–38). Exposure of PSCs to UV light at 300–338 nm elicits a transient blue–green fluorescence that can be quantitated (11). Upon inflammatory stimulation from the environment, these cells become activated, "losing" their retinoid containing lipid droplets and become myofibroblastic, secreting αSMA. Even though a number of studies have been focused on the biology of the PSCs and their activation, the mechanism of loss of retinoids has not been studied in PSCs as they have been studied in HSCs. In HSCs, activation leads to the metabolism of retinol to retinoic acid, which acts as a ligand for the RAR/RXR signaling pathway. This pathway is one of the key pathways involved in differentiation and is very tightly regulated. Upon activation, the RAR/RXR bind to their response elements (RARE) in the promoter of specific genes and regulate transcription of genes involved in differentiation, proliferation, and survival. One such pathway stimulated by the RAR/RXR is the TGFβ signaling pathway.

It is classically believed that resident fibroblasts in any tissue become activated during wound healing and revert to their inactive state upon resolution (14). However, when associated with TECs, this activation often becomes irreversible, leading to formation of CAFs. In the pancreas, an injury or insult leads to activation of the PSCs. During the course of pancreatic tumor progression, the PSCs become activated by the TECs and reach a stage where they presumably become irreversibly activated and drive tumor growth. At this point, they express fibroblast activation protein and fibroblast secretory protein and become CAFs that cannot go back to the quiescent stage. Thus, targeting the CAFs at this stage with molecules that can revert the back to "quiescent" state can be considered an attractive therapeutic strategy, as this will disrupt the tumor–stroma cross-talk and inhibit the tumor growth and progression.

Our transcriptomics data showed that treatment of CAFs (isolated from a mature KPC mouse tumor) with triptolide deregulated the TGFβ pathway and the RAR/RXR signaling pathway (Fig. 2; Supplementary Fig. S4). Interestingly, the expression of RBP was increased by this analysis and the expression of RDH was downregulated. This indicated that triptolide was affecting the retinol-metabolizing pathway. Instead of the retinol being metabolized to RA (by RDH), there was more retinol in the CAFs that needed stabilization by RBPs. This was confirmed by both our Oil Red staining and vitamin A accumulation assay (Fig. 4). We further observed, this could be that the RAR/RXR pathway is a key developmental and differentiation pathway in the cells, it is very tightly regulated. While retinoic acid (ATRA and 9cisRA) can stimulate the RAR/RXR transcriptional activity, an excess of it acts as an inhibitor of RDH and shuts down the conversion of retinol to RA. A number of studies have shown that ATRA can prevent activation of PSCs and this only observed at high doses (39, 40). Our studies showed that treatment with ATRA at a low dose increased proliferation of CAFs, while at an increased dose of 1 μmol/L, it inhibited proliferation presumably by causing a feedback inhibition of the RAR/RXR pathway (Supplementary Fig. S5).

Previous work from our laboratory has shown that Minnelide, the water-soluble prodrug of triptolide, is an effective antitumor and antistromal compound (6). At a dose of 0.4 mg/kg, Minnelide depletes the stroma, induces stromal and tumor cell death, and prevents metastasis. However, our recently completed phase I clinical trial shows that the MTD of Minnelide in patients in 0.67 mg/m^2, which translates to

0.2 mg/kg in mice. At this dose, Minnelide still decreases the ECM in the stroma, but does not have any profound effect on viability of TECs or CAFs. In this work, we show that while CAFs promoted tumor growth and invasion, treatment with Minnelide did not significantly decrease metastasis *in vivo* (Fig. 1). However, treatment with Minnelide did result in less number of proliferating cells in the tumor as was seen by BrdUrd uptake (Fig. 1; Supplementary Fig. S2). This effect was confirmed *in vitro* as well, where treatment with CM from triptolide-treated CAFs decreased proliferation of TECs as well as CAFs (Fig. 4A).

It is well known that CAFs produce TGFβ, which in turn activates oncogenic signaling in the tumor epithelial cells via the SMAD group of transcription factors (23, 24). It is also known that TGFβ signaling leads to induction of Sp1 transcriptional activity in tumors (25). Although Sp1 is not present is terminally differentiated tissues, we and others have seen that pancreatic cancer has an increased Sp1 activity[26] and its inhibition leads to cancer cell death. Our data suggest that triptolide treatment of CAFs leads to inhibition of TGFβ mRNA levels as well as its secretion (Fig. 3). Upon treating MIA PaCa-2 cells with CM from 25 nmol/L triptolide-treated PSCs, we saw a distinct decrease in the SMAD transcriptional activity (Fig. 6), Sp1 expression, as well as Sp1 activity (Fig. 6). In addition, other antiapoptotic pathways that are known to be upregulated in pancreatic cancer (and regulated by Sp1 activity) were also found to be downregulated.

In addition to decreased proliferation, treatment with triptolide also decreased ECM secretion by CAFs. Interestingly, all the "inhibition" effect of triptolide was recovered upon treatment with TGFβ, which indicated that triptolide-induced inactivation of CAFs led to a decreased TGFβ secretion by these cells, which deregulated both the autocrine signaling in the CAFs as well as the paracrine signaling in the TECs. This has been demonstrated in the schematic figure (Fig. 7).

Conclusion

The role of CAFs in promoting tumor growth and invasion has been established in a number of cancers including pancreatic cancer. Several studies in pancreatic cancer have also been focused on depletion of stromal components specifically the ECM. In the current study, we show for the first time that Minnelide, and its active compound triptolide, is able to revert the presumably "irreversible" CAFs to an inactive state, where they show decreased TGFβ secretion and less ECM production. This in turn, affects the TECs and lowers their proliferation, decreases their oncogenic signaling, leading to a tumor regression. This mechanistic insight on the effect of triptolide on CAF inactivation will pave the way for developing viable and attractive therapy for pancreatic cancer, a disease that still lacks efficient chemotherapeutic options.

Disclosure of Potential Conflicts of Interest

S. Banerjee is a consultant/advisory board member for Minneamrita Therapeutics. A. Saluja is a chief scientific officer, reports receiving a commercial research grant, and has ownership interest (including patents) in Minneamrita Therapeutics. No potential conflicts of interest were disclosed by the other authors.

Authors' Contributions

Conception and design: P. Dauer, V.K. Gupta, N.S. Sharma, S.M. Vickers, S. Banerjee, A. Saluja
Development of methodology: P. Dauer, X. Zhao, V.K. Gupta, N.S. Sharma, V. Dudeja, S. Banerjee, A. Saluja
Acquisition of data (provided animals, acquired and managed patients, provided facilities, etc.): P. Dauer, X. Zhao, V.K. Gupta, N.S. Sharma, K. Kesh, P. Gnamlin, V. Dudeja
Analysis and interpretation of data (e.g., statistical analysis, biostatistics, computational analysis): P. Dauer, X. Zhao, V.K. Gupta, N.S. Sharma, K. Kesh, P. Gnamlin, V. Dudeja, S. Banerjee, A. Saluja
Writing, review, and/or revision of the manuscript: P. Dauer, X. Zhao, V.K. Gupta, N.S. Sharma, K. Kesh, P. Gnamlin, V. Dudeja, S. Banerjee, A. Saluja
Administrative, technical, or material support (i.e., reporting or organizing data, constructing databases): P. Dauer, S. Banerjee, A. Saluja
Study supervision: S. Banerjee, A. Saluja

Acknowledgments

This study was funded by NIH grants R01-CA170946 and CA124723 (to A. Saluja); NIH grant R01-CA184274 (to S. Banerjee); Katherine and Robert Goodale foundation support (to A. Saluja), and Minneamrita Therapeutics LLC (to A. Saluja). The authors would also like to acknowledge the Flow Cytometry Core and the Analytical Imaging Core of the Sylvester Comprehensive Cancer Center for their help and support with the experiments.

The costs of publication of this article were defrayed in part by the payment of page charges. This article must therefore be hereby marked *advertisement* in accordance with 18 U.S.C. Section 1734 solely to indicate this fact.

Received August 6, 2017; revised September 29, 2017; accepted December 14, 2017; published OnlineFirst December 19, 2017.

References

1. Jemal A, Bray F, Center MM, Ferlay J, Ward E, Forman D. Global cancer statistics. CA: Cancer J Clin 2011;61:69–90.
2. Hamada S, Masamune A, Shimosegawa T. Novel therapeutic strategies targeting tumor-stromal interactions in pancreatic cancer. Front Physiol 2013;4:331.
3. Hidalgo M. Pancreatic cancer. N Engl J Med 2010;362:1605–17.
4. Jacobetz MA, Chan DS, Neesse A, Bapiro TE, Cook N, Frese KK, et al. Hyaluronan impairs vascular function and drug delivery in a mouse model of pancreatic cancer. Gut 2013;62:112–20.
5. Provenzano PP, Cuevas C, Chang AE, Goel VK, Von Hoff DD, Hingorani SR. Enzymatic targeting of the stroma ablates physical barriers to treatment of pancreatic ductal adenocarcinoma. Cancer Cell 2012; 21:418–29.
6. Banerjee S, Modi S, McGinn O, Zhao X, Dudeja V, Ramakrishnan S, et al. Impaired synthesis of stromal components in response to Minnelide improves vascular function, drug delivery and survival in pancreatic cancer. Clin Cancer Res 2016;22:415–25.
7. Rhim AD, Oberstein PE, Thomas DH, Mirek ET, Palermo CF, Sastra SA, et al. Stromal elements act to restrain, rather than support, pancreatic ductal adenocarcinoma. Cancer Cell 2014;25:735–47.
8. Khan S, Ebeling MC, Chauhan N, Thompson PA, Gara RK, Ganju A, et al. Ormeloxifene suppresses desmoplasia and enhances sensitivity of gemcitabine in pancreatic cancer. Cancer Res 2015;75:2292–304.
9. Neesse A, Michl P, Frese KK, Feig C, Cook N, Jacobetz MA, et al. Stromal biology and therapy in pancreatic cancer. Gut 2011;60:861–8.
10. Neesse A, Algul H, Tuveson DA, Gress TM. Stromal biology and therapy in pancreatic cancer: a changing paradigm. Gut 2015;64:1476–84.
11. Apte MV, Xu Z, Pothula S, Goldstein D, Pirola RC, Wilson JS. Pancreatic cancer: The microenvironment needs attention too! Pancreatology 2015; 15:S32–8.
12. Heinemann V, Reni M, Ychou M, Richel DJ, Macarulla T, Ducreux M. Tumour-stroma interactions in pancreatic ductal adenocarcinoma: rationale and current evidence for new therapeutic strategies. Cancer Treat Rev 2014;40:118–28.

13. Lunardi S, Muschel RJ, Brunner TB. The stromal compartments in pancreatic cancer: are there any therapeutic targets? Cancer Lett 2014; 343:147–55.
14. Kalluri R. The biology and function of fibroblasts in cancer. Nat Rev Cancer 2016;16:582–98.
15. Sherman MH, Yu RT, Engle DD, Ding N, Atkins AR, Tiriac H, et al. Vitamin D receptor-mediated stromal reprogramming suppresses pancreatitis and enhances pancreatic cancer therapy. Cell 2014;159: 80–93.
16. Phillips PA, Dudeja V, McCarroll JA, Borja-Cacho D, Dawra RK, Grizzle WE, et al. Triptolide induces pancreatic cancer cell death via inhibition of heat shock protein 70. Cancer Res 2007;67:9407–16.
17. Chugh R, Sangwan V, Patil SP, Dudeja V, Dawra RK, Banerjee S, et al. A preclinical evaluation of minnelide as a therapeutic agent against pancreatic cancer. Sci Transl Med 2012;4:156ra39.
18. Alsaied OA, Sangwan V, Banerjee S, Krosch TC, Chugh R, Saluja A, et al. Sorafenib and triptolide as combination therapy for hepatocellular carcinoma. Surgery 2014;156:270–9.
19. Antonoff MB, Chugh R, Borja-Cacho D, Dudeja V, Clawson KA, Skube SJ, et al. Triptolide therapy for neuroblastoma decreases cell viability in vitro and inhibits tumor growth in vivo. Surgery 2009;146:282–90.
20. Banerjee S, Saluja A. Minnelide, a novel drug for pancreatic and liver cancer. Pancreatology 2015;15:S39–43.
21. Banerjee S, Thayanithy V, Sangwan V, Mackenzie TN, Saluja AK, Subramanian S. Minnelide reduces tumor burden in preclinical models of osteosarcoma. Cancer Lett 2013;335:412–20.
22. Sangwan V, Banerjee S, Jensen KM, Chen Z, Chugh R, Dudeja V, et al. Primary and liver metastasis-derived cell lines from KrasG12D; Trp53R172H; Pdx-1 Cre animals undergo apoptosis in response to triptolide. Pancreas 2015;44:583–9.
23. Banerjee S, Sangwan V, McGinn O, Chugh R, Dudeja V, Vickers SM, et al. Triptolide-induced cell death in pancreatic cancer is mediated by O-GlcNAc modification of transcription factor Sp1. J Biol Chem 2013;288: 33927–38.
24. Dudeja V, Mujumdar N, Phillips P, Chugh R, Borja-Cacho D, Dawra RK, et al. Heat shock protein 70 inhibits apoptosis in cancer cells through simultaneous and independent mechanisms. Gastroenterology 2009;136: 1772–82.
25. Greeno E, Borazanci E, Gockerman J, Korn R, Saluja A, Von Hoff D. Phase I dose escalation and pharmacokinetic study of 14-O-phosphonooxymethyltriptolide. AACR Annual Meeting 2015 Apr 18–22.
26. Sharon Y, Alon L, Glanz S, Servais C, Erez N. Isolation of normal and cancer-associated fibroblasts from fresh tissues by fluorescence activated cell sorting (FACS). J Vis Exp 2013:e4425.
27. Andrews S. FastQC: a quality control tool for high throughput sequence data; 2010. Available at http://www.bioinformatics.babraham.ac.uk/projects/fastqc.
28. Trapnell C, Pachter L, Salzberg SL. TopHat: discovering splice junctions with RNA-Seq. Bioinformatics 2009;25:1105–11.
29. Trapnell C, Roberts A, Goff L, Pertea G, Kim D, Kelley DR, et al. Differential gene and transcript expression analysis of RNA-seq experiments with TopHat and Cufflinks. Nat Protoc 2012;7:562–78.
30. Goff LA, Trapnell C, Kelley D. CummeRbund: analysis, exploration, manipulation, and visualization of Cufflinks high-throughput sequencing data. 2.10.0: R package; 2013. Available at http://bioconductor.org/packages/release/bioc/html/cummeRbund.html.
31. Yu G, Wang LG, Han Y, He QY. clusterProfiler: an R package for comparing biological themes among gene clusters. Omics 2012;16:284–7.
32. Subramanian A, Tamayo P, Mootha VK, Mukherjee S, Ebert BL, Gillette MA, et al. Gene set enrichment analysis: a knowledge-based approach for interpreting genome-wide expression profiles. Proc Nat Acad Sci U S A 2005;102:15545–50.
33. Jungert K, Buck A, von Wichert G, Adler G, Konig A, Buchholz M, et al. Sp1 is required for transforming growth factor-beta-induced mesenchymal transition and migration in pancreatic cancer cells. Cancer Res 2007;67:1563–70.
34. Koo BH, Kim Y, Cho YJ, Kim DS. Distinct roles of transforming growth factor-beta signaling and transforming growth factor-beta receptor inhibitor SB431542 in the regulation of p21 expression. Eur J Pharmacol 2015;764:413–23.
35. Pardali K, Kurisaki A, Moren A, ten Dijke P, Kardassis D, Moustakas A. Role of Smad proteins and transcription factor Sp1 in p21(Waf1/Cip1) regulation by transforming growth factor-beta. J Biol Chem 2000;275: 29244–56.
36. Apte MV, Pirola RC, Wilson JS. Pancreatic stellate cells: a starring role in normal and diseased pancreas. Front Physiol 2012;3:344.
37. Apte MV, Wilson JS. Dangerous liaisons: pancreatic stellate cells and pancreatic cancer cells. J Gastroenterol Hepatol 2012;27:69–74.
38. McCarroll JA, Naim S, Sharbeen G, Russia N, Lee J, Kavallaris M, et al. Role of pancreatic stellate cells in chemoresistance in pancreatic cancer. Front Physiol 2014;5:141.
39. Chronopoulos A, Robinson B, Sarper M, Cortes E, Auernheimer V, Lachowski D, et al. ATRA mechanically reprograms pancreatic stellate cells to suppress matrix remodelling and inhibit cancer cell invasion. Nat Commun 2016;7:12630.
40. Sarper M, Cortes E, Lieberthal TJ, Del Rio Hernandez A. ATRA modulates mechanical activation of TGF-beta by pancreatic stellate cells. Sci Rep 2016;6:27639.